Proceedings of:
8th International Congress of Fluid Dynamics & Propulsion
December 14-17, 2006, Sharm El-Shiekh, Sinai, Egypt.

ICFDP 8-EG-151

ON THE CRITICAL REYNOLDS NUMBER FOR VORTEX SHEDDING PAST BLUFF BODIES

K.A. Elshorbagy, E.M. Wahba and R.S. Afify
Mechanical Engineering Department, Alexandria University
Alexandria, EGYPT 21544
E-mail: emwahba@yahoo.com

ABSTRACT

In the present study, a numerical approach is adopted to analyze the flow past bluff bodies. Four basic bluff body shapes are considered, namely circular, square, triangular and T-shaped cylinders. For each of these bluff bodies, the flow is simulated in the Reynolds number range of ($\mathrm{Re} \leq 200$). For low Reynolds numbers, the flow is steady and a separated region is visible in the wake. The size of the separated region increases with increasing Reynolds number for all four shapes. At a certain critical Reynolds number, the steady flow past the bluff body becomes unstable and the flow bifurcates to an unsteady state. The critical Reynolds number for each shape is evaluated and the effect of bluff body geometry on this critical Reynolds number is identified. Moreover, as the Reynolds number is further increased, vortices are shed in the wake of all four bodies. The Strouhal number for such vortex shedding phenomena is calculated and the effect of the bluff body shape on the value of this number is clarified.

INTRODUCTION

The study of the dynamics of fluid flow past bluff bodies is a problem of great practical importance. Such a flow field is frequently encountered in engineering applications such as the flow over aircrafts, submarines, offshore pipelines, tall buildings, chimneys, bridges and cables. The flow field is extremely difficult to study analytically due to the presence of complex flow phenomena such as separation, instabilities, bifurcation and vortex shedding.

Various studies were conducted on the flow past bluff bodies. These studies revealed that the characteristics of the flow field are mainly governed by the flow Reynolds number. Other influencing parameters include blockage effects, three-dimensional effects and the bluff body shape.

Sohankar et al (1) performed numerical simulation of laminar unsteady two-dimensional flow around a square cylinder at zero angle of attack in low Re range ($45 \leq \mathrm{Re} \leq 250$). They extended their study in (2) and considered an angle of attack in the range ($0^o \leq \alpha \leq 90^o$) for Re = 100 and 200. Moreover, in (3) they performed the numerical simulation of laminar unsteady two-dimensional flow around a square cylinder at incidence ($0^o \leq \alpha \leq 45^o$) for low Reynolds numbers ($45 \leq \mathrm{Re} \leq 200$). The calculations predicted a Von Karman vortex sheet behind the cylinder that agreed well with experimental results. They also investigated the onset of vortex shedding using the Stuart-Landau equation at various angles of incidence and for a solid blockage of 5%.

Young et al (4) simulated vortex shedding past a single circular cylinder and flow past two cylinders in which one acts as a control cylinder, for low Reynolds numbers flow ($\mathrm{Re} \leq 140$). More recently, an efficient method for simulating the 2D steady and unsteady incompressible flows past circular cylinders was described by Ding et al (5). The method is a hybrid approach, which combines the conventional finite difference (FD) scheme and the mesh free least square-based finite difference (MLSFD) method. It is also adopted to deal with complex geometries.

For a triangular bluff body, Frank et al (6) investigated a dual equilateral triangular bluff body vortex shedding flow meter using oscillating outlet boundary conditions by implementing a user defined function in FLUENT. Their results showed that the dual body arrangement affected the frequency and amplitude of the vortex shedding phenomena.

For T-shape cylinders, Miau et al (7) developed a configuration of a T-shaped vortex shedder to improve the quality of the measured vortex-shedding signal for vortex flow meters. This T-shaped vortex shedder comprises a trapezoidal cylinder, which is fixed in shape, and an extended plate attached behind the cylinder, whose length is variable.

Alternative studies considered the flow over a combination of bluff bodies. Mittal et al (8) examined the flow past a pair of equal diameter circular cylinders in tandem and staggered arrangements using a stabilized finite element formulation. They observed that the qualitative nature of the flow depends strongly on both the arrangement of cylinders and the Reynolds number. They also found that in all cases, when the flow becomes unsteady, the downstream cylinder, which lies in the wake of the upstream one, experiences very large unsteady forces that may lead to wake-induced flutter. The Strouhal number based on the dominant frequency attains the same value for both cylinders. Summer et al (9, 10) conducted similar studies in a staggered configuration in cross flow with incidence angles varying from α = 0° to 90° and the aerodynamic forces were measured on both the upstream and downstream cylinders.

For the three-dimensional studies, Sohankar et al (11) numerically simulated the unsteady flow over a square cylinder in the Reynolds number range ($200 \le Re \le 500$). They found that the mean time flow patterns are not perfectly symmetric for Re > 300 with respect to the incoming flow. They also noted that there is a marked characteristic pulsation in the force components in the three-dimensional flow for Re > 300.

In the present study, the flow past square, circular, triangular and T-shaped cylinders are simulated in order to examine the effect of the bluff body shape on the characteristics of the flow field.

NOMENCLATURE

A Frontal area, m^2.
C_l Lift coefficient
(C_l = Lift force / $0.5\rho U^2 A$), dimensionless.
C_d Drag coefficient
(C_d = Drag force / $0.5\rho U^2 A$), dimensionless.
d Bluff body's frontal length, m.
f Shedding frequency, 1/sec.
H Domain length, m.
L Length of recirculating zone, m.
N.S.E Navier Stokes Equations
P pressure, N/m^2.
Re Reynolds number (Re = U d / ν), dimensionless.
Re_{cr} Critical Reynolds number, dimensionless.
St Strouhal number (St = f d / U), dimensionless.
U Uniform free stream velocity, m/s.
u Velocity component in x-direction, m/s.
v Velocity component in y-direction, m/s.
w Velocity component in z-direction, m/s.
X Body force in x-direction, N/kg.
X_u The upstream distance, m.
X_d The downstream distance, m.
Y Body force in y-direction, N/kg.
Z Body force in z-direction, N/kg.
ρ Density, kg / m^3.
μ Dynamic viscosity, N.s/m^2.
ν Kinematic viscosity, m^2/s.

NUMERICAL METHODS

1 FLOW DOMAIN AND BOUNDARY CONDITIONS

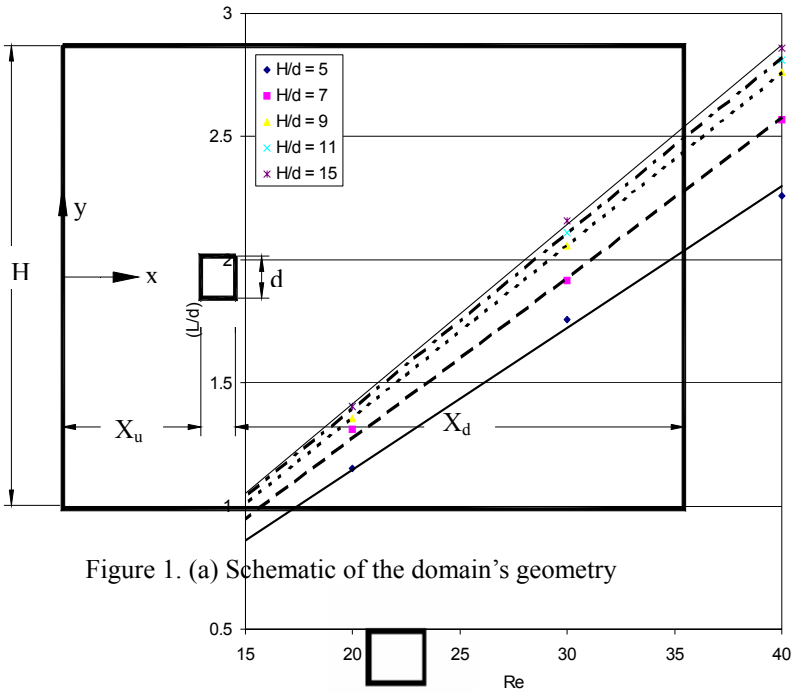

Figure 1. (a) Schematic of the domain's geometry

Figure 3. Effect of width (H) on the length of the re-circulating zone

(b) Bluff body shapes used

The problem to be considered is shown schematically in figure 1. The domain's width and length are (X_u + d + X_d) and H respectively. All dimensions are scaled to frontal length d. The bluff body location in the domain is as shown. The bluff body shapes considered are shown in figure 1(b) all with the same frontal length (d). At the left boundary the inflow is a rectilinear uniform flow, which enters the domain aligned with x-axis with a velocity (u = U and v = 0). The upper and lower boundaries have the same velocity as the inflow. The entire bluff body boundaries are considered as walls at which the no-

slip condition is applied. Reynolds number is varied by varying the free stream velocity (U).

The values of X_u, H, X_d are chosen to ensure domain independent results. To reach this condition, several

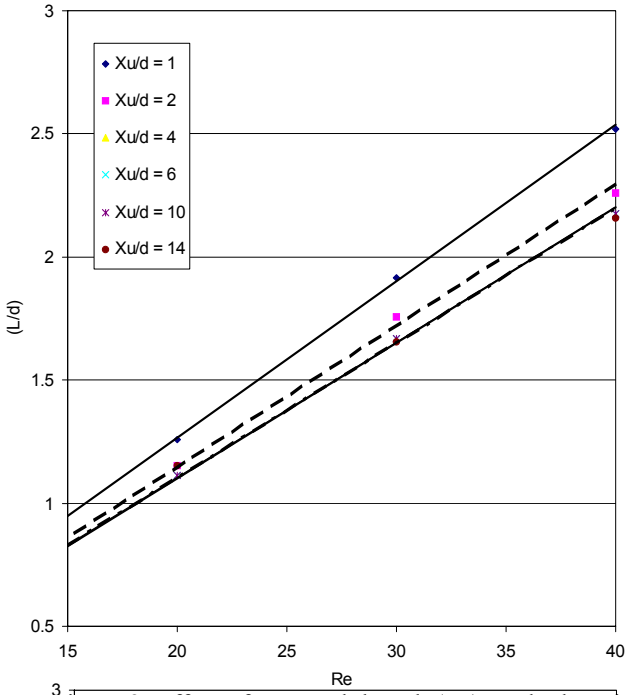

Figure 3. Effect of approach length (X_u) on the length of the re-circulating zone

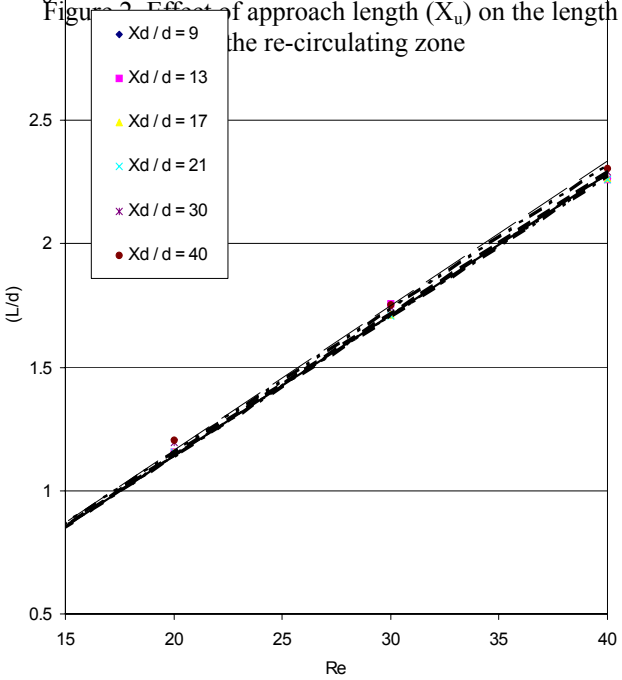

Figure 4. Effect of down stream (X_d) on the length of the re-circulating zone

simulations are performed for flow past a square cylinder. The results of the simulations are given in figures (2) to (4). In figure (2), the relation between the length of the recirculation zone (L/d) and the Reynolds number is plotted for different values of X_u. As can be seen, after a certain value of X_u, the results became independent of the upstream distance (X_u).

Similar results are reported in figure (3) and (4) for the dimensions (H) and (X_d) respectively. Based on the above results, the following non-dimensional values for X_u, H, X_d are selected to ensure a domain that provide results independent of its dimensions.

$X_u/d = 5$, $X_d/d = 15$, $H/d = 15$

Moreover, the above non-dimensional values for X_u, H, X_d agreed well with those reported in references (3, 4, 5 and 23).

2 STREAM FUNCTION-VORTICITY FORMULATION

The incompressible N.S.E. can be re-written in terms of a stream function-vorticity formulation as follows:

$$\left.\begin{aligned} \frac{\partial \xi}{\partial t} + u\frac{\partial \xi}{\partial x} + v\frac{\partial \xi}{\partial y} &= \upsilon\left(\frac{\partial^2 \xi}{\partial x^2} + \frac{\partial^2 \xi}{\partial y^2}\right) \\ \frac{\partial^2 \psi}{\partial x^2} + \frac{\partial^2 \psi}{\partial y^2} &= -\xi \end{aligned}\right\} \quad (1)$$

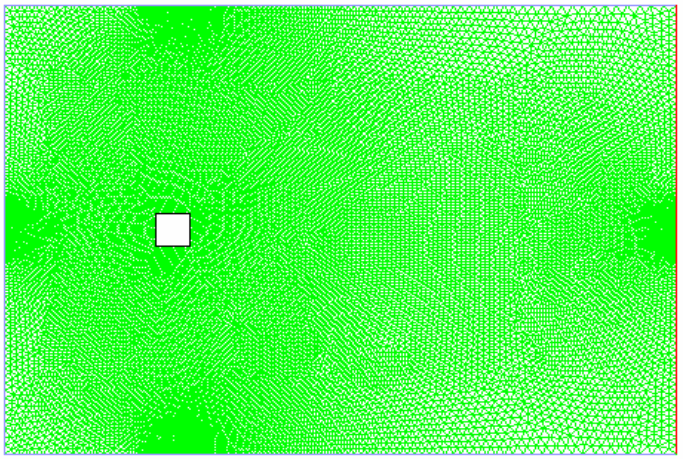

Figure 5 Geometry of the domain with a square bluff body and clustering triangular mesh

Where $\xi = \frac{\partial v}{\partial x} - \frac{\partial u}{\partial y}$

$$\frac{\partial \psi}{\partial y} = u \;\&\; \frac{\partial \psi}{\partial x} = -v$$

$\frac{\partial \xi}{\partial t}$ is an artificial time dependent term, which is added to the vorticity equation to enhance numerical stability. A first order time integration is used to advance the equations in the artificial time representing the iterations.

The stream function-vorticity formulation is used to simulate the flow past a square cylinder. A body fitted co-

ordinate system is used to generate the grid around the square cylinder.

A central-based finite difference scheme of second order accuracy is used to discretize the governing equations resulting in the following system of algebraic equations:

$$\left.\begin{aligned}
&\frac{\xi_{i,j}-\xi_{i,j}^{n-1}}{\Delta t}+u_{i,j}\frac{\xi_{i+1,j}-\xi_{i-1,j}}{2\Delta x}+v\frac{\xi_{i,j+1}-\xi_{i,j-1}}{2\Delta y}\\
&=\nu\left(\frac{\xi_{i+1,j}-2\xi_{i,j}+\xi_{i-1,j}}{\Delta x^2}+\frac{\xi_{i,j+1}-2\xi_{i,j}+\xi_{i,j-1}}{\Delta y^2}\right)\\
&\frac{\psi_{i+1,j}-2\psi_{i,j}+\psi_{i-1,j}}{\Delta x^2}+\frac{\psi_{i,j+1}-2\psi_{i,j}+\psi_{i,j-1}}{\Delta y^2}=-\xi_{i,j}
\end{aligned}\right\} \quad (2)$$

The discretized stream function equation is solved using a line successive over-relaxation scheme (LSOR) while the vorticity transport equation is solved using a local time stepping procedure. The above scheme is only used to simulate the flow past a square cylinder. For other bluff body shapes, a commercial CFD software package is used as stated in the following section.

3 COMMERCIAL CFD SOFTWARE PACKAGE

The commercial software package FLUENT is used to simulate the flow past the considered bluff bodies.

In figure 5, it is seen that triangular cells are used for the domain. The number of elements in each shape is as follows:

Shape	**No. of elements**
Square	31222
Circle	33614
Triangle	34290
T-shape	31324
Inverted Triangle	33900

A segregated solver is used in conjunction with an implicit formulation. The boundary conditions are uniform flow at the inflow and the upper and lower boundaries. The no slip condition is applied at the bluff body surface.

NUMERICAL RESULTS AND DISCUSSION

The results for each shape are divided into three categories as follow:

1 THE RELATION BETWEEN RE AND THE (L/d) IN LAMINAR STEADY FLOW

For low Reynolds numbers, the flow past a bluff body is steady with a separated region in the wake. The length of this separated region increases as Reynolds number increases. As shown in figure (6) all the shapes have the same trend in which the vortex length increases as the Reynolds number increases but with different values for each shape as shown in the table (1).

Table 1. Vortex length for different shapes

Re \ Shape	Vortex length (L/d)					
	ψ - ξ	FLUENT				
	Square	Square	Circle	Triangle	Inverted Tri.	T shape
10	0.65	0.638	0.247	0.0	0.759	0.0
15	0.95	0.957	0.598	0.437	1.106	0.209
20	1.25	1.278	0.914	0.899	1.417	0.771
25	1.5	1.69	1.247	1.247	1.737	1.252
30	1.8	2.013	1.595	2.006	2.119	1.782
35	2.1	2.44	1.892	2.608	2.473	2.341
40	2.35	2.677	2.202	--	--	--

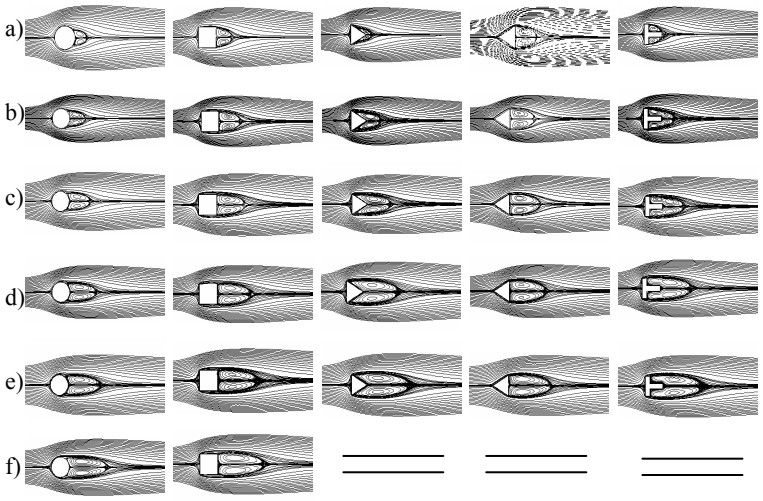

Figure 6. Vortex length for different shapes at various values of Re
a) Re = 15 b) Re = 20 c) Re = 25 d) Re = 30 e) Re = 35 f) Re = 40

In the case of flow past a circular cylinder, separation occurs due to adverse pressure gradient in the downstream direction, resulting in back and forth movement of the separation point on the cylinder surface. However, in the cases of the flow past a rectangle, triangle and T-shape cylinder, the location of flow separation is fixed at upstream corners of the cylinder due to the abrupt geometrical change (12).

In all cases, a pair of symmetric vortices develops behind the bluff body and is perfectly aligned. These vortices become larger and also the length of the re-circulation zone as Reynolds number increases, as seen in figure (7).

Table 2. Comparison between results of vortex length (L/d) for the flow over a circular cylinder at different Reynolds numbers.

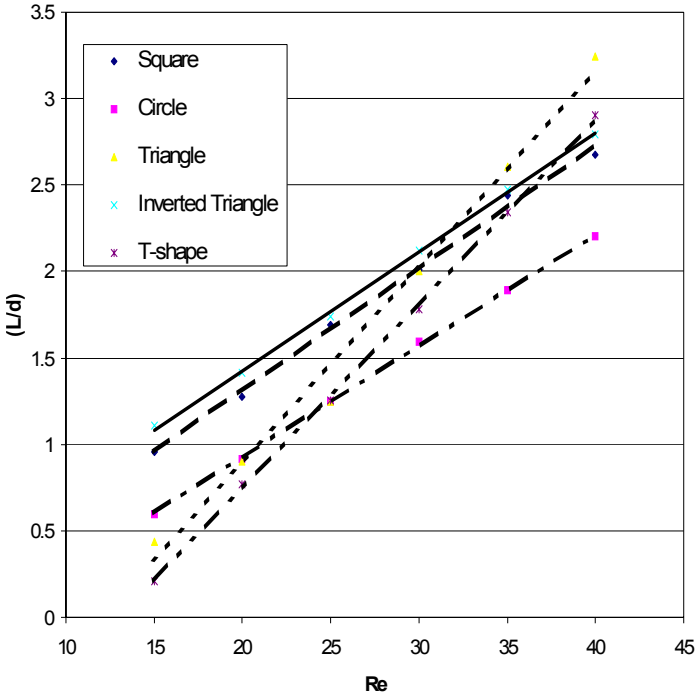

Figure 7. Vortex length for different

Re	10	20	40
Present study	0.247	0.914	2.202
Dannis et al (13)	0.252	0.94	2.35
Takami et al (14)	0.249	0.935	2.32
Tuann et al (15)	0.25	0.9	2.1
Fornberg et al (16)	--	0.91	2.24
Ding et al (5)	0.252	0.93	2.20

As shown in table 2, the vortex length values at different Reynolds numbers of the present study are in a good agreement with the previous studies.

2 THE CRITICAL REYNOLDS NUMBER

The critical Reynolds number is the number at which the flow bifurcates from a steady state to an unsteady state. To calculate the critical Reynolds number, numerous simulations are performed for different values of Reynolds number and the lift coefficient is monitored. The critical Reynolds number is identified as the lowest Reynolds number value at which the lift coefficient is no longer steady and starts varying periodically with time.

Table 3. Results for values of the critical Reynolds number Re_{cr} from the present study for different shapes in comparison with available results from other sources.

Shape	Re_{cr}	Source
Circle	46	Present study
	46	Hu et al (17)
Square	45	Present study
	50	Sohankar et al (blockage = 14.2 %) (3)
	$40 < Re_{cr} < 55$	Sohankar et al (Stuart-Landau equation) (3)
	47 ± 2	Norborg et al (18)
	53	Kelkar and Patankar (19)
Triangle	37	Present study
	39.9	Kumar et al (20)
Inverted Triangle	39	Present study
T-shape	38	Present study

As shown in table 3, there is also a good agreement between the value of the critical Reynolds numbers of the present study and the previous studies. It is, however, clear that the critical Reynolds number varies slightly with the geometry as its value, in the present study, lies between 37 and 46 for the basic shapes.

3 RELATION BETWEEN REYNOLDS NUMBER (Re) AND STROUHAL NUMBER (St) IN LAMINAR UNSTEADY FLOW

For Reynolds numbers higher than the critical value, vortex shedding starts to appear in the wake of the bluff body, where vortices are shed alternatively from both sides of the body at a shedding frequency defined by the Strouhal number.

Table 4. Values of St for Re = 100 and 200 for different bluff body shapes.

Re \ Shape	Strouhal Number (St)				
	Square	Circle	Triangle	Inverted Tri	T shape
100	0.1523	0.175	0.164	0.21	0.1516
200	0.156	0.206	0.177	0.221	0.168

As shown in table 4, Strouhal Number increases as Reynolds number increases for all shapes considered.

It is clear from table (5) that excellent agreement has been achieved between the values of Strouhal number of the present study and other authors.

Table 5. Comparisons at Re = 100 using Strouhal number for circle and square shapes.

Shape	St	Author	Comment
Circle	0.175	Present study	Grid = 120 x 90
	0.168	D.L.Young et al. (4)	Grid = 5750
	0.165	D.L.Young et al. (4)	Grid = 1802
	0.18	Gresho et al. (21)	Grid = 1852 (numerical)
	0.164	H. Ding et al. (5)	--
	0.163	Li et al. (22)	--
	0.160	Braza et al. (23)	--
	0.182	White (24)	The value of the St is obtained from a graph
Square	0.1523	Present study	Grid = 120 x 90
	0.150	Sohankar et al. (3)	Xd = 10
	0.146	Sohankar et al. (3)	Grid = 210 x 202
	0.146	Sohankar et al. (3)	Grid = 96 x 94

	0.139	Yih-Jena Jan et al. (25)	del (t) = 0.04
	0.144	Yih-Jena Jan et al. (25)	del (t) = 0.01
	0.135-0.140	Okajima (26)	Experimental
	0.154	Davis et al (27)	Numerical

Figures (7) to (11) show the time dependent behavior of streamlines and vorticity at Re = 100 for the different bluff body shapes. It is clear that the periodicity of the flow field has been successfully revealed in all of the shapes. Lift coefficient at the surface of the bluff body is also given, its value oscillating around zero for all the cases.

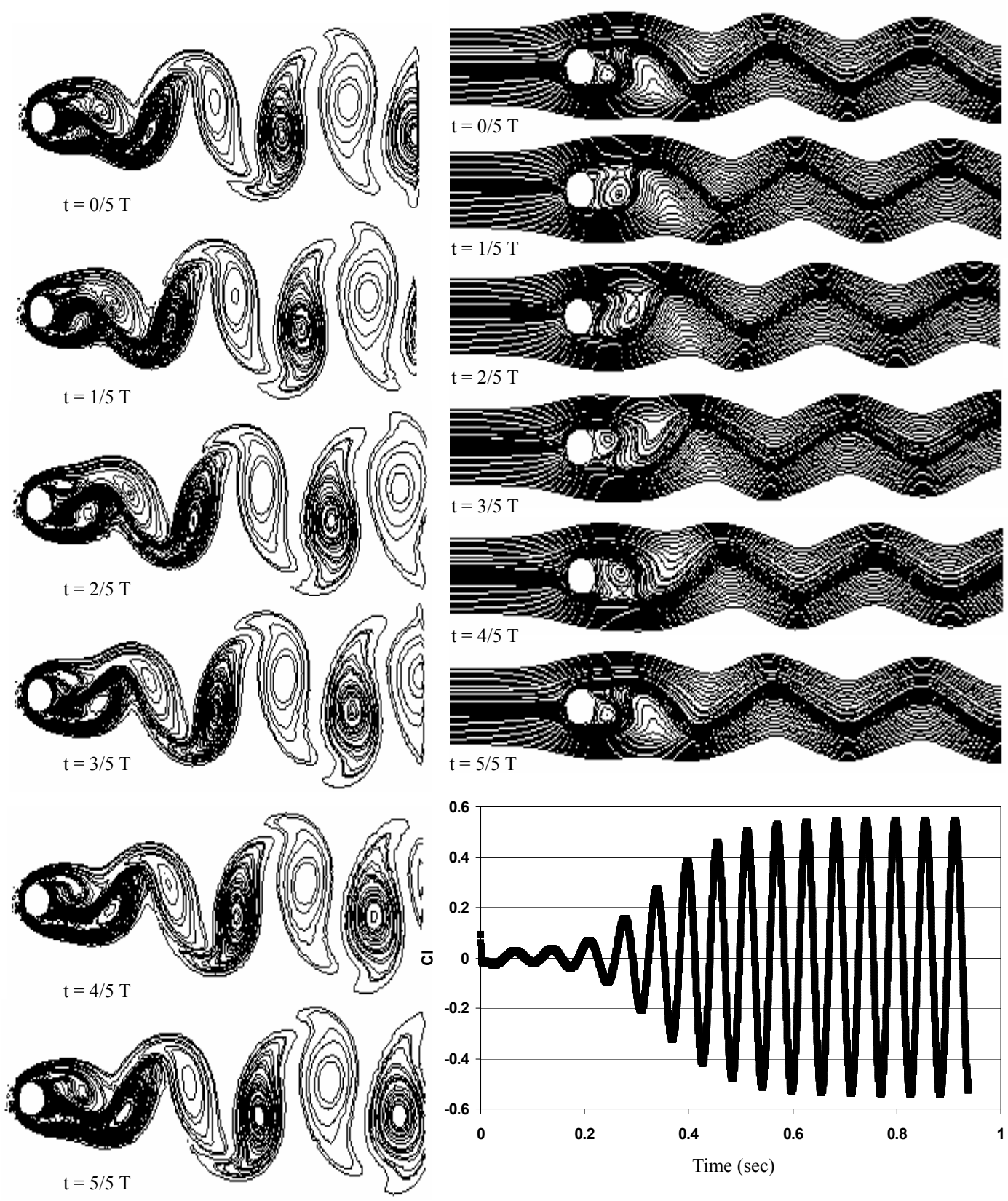

Lift coefficient versus time for a circle shape

Figure 7. Time evolution of vortex shedding streamline plots and vorticity contours for flow passing a circular cylinder at Re = 100

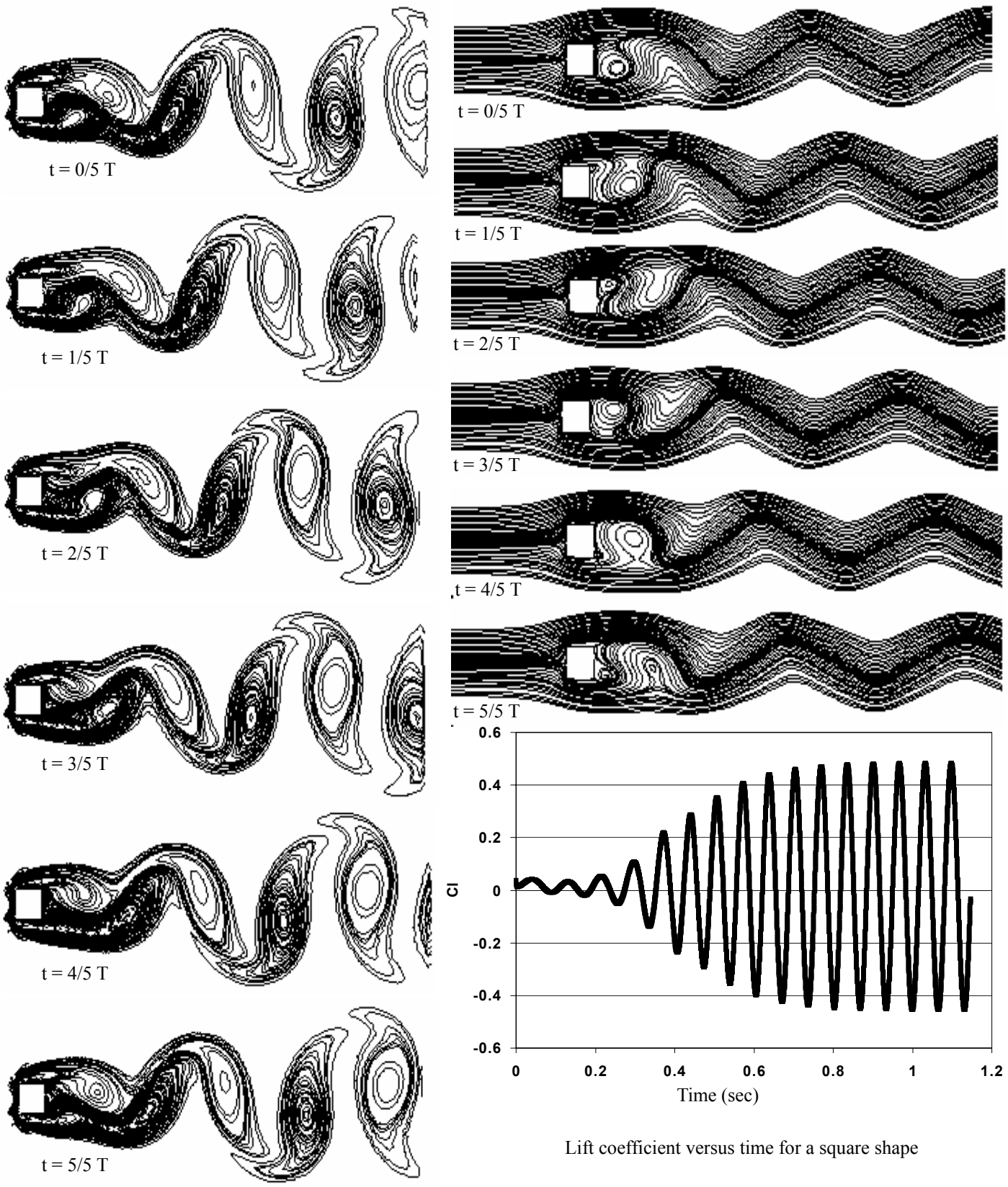

Lift coefficient versus time for a square shape

Figure 8. Time evolution of vortex shedding streamline plots and vorticity contours for flow passing a square cylinder at Re = 100

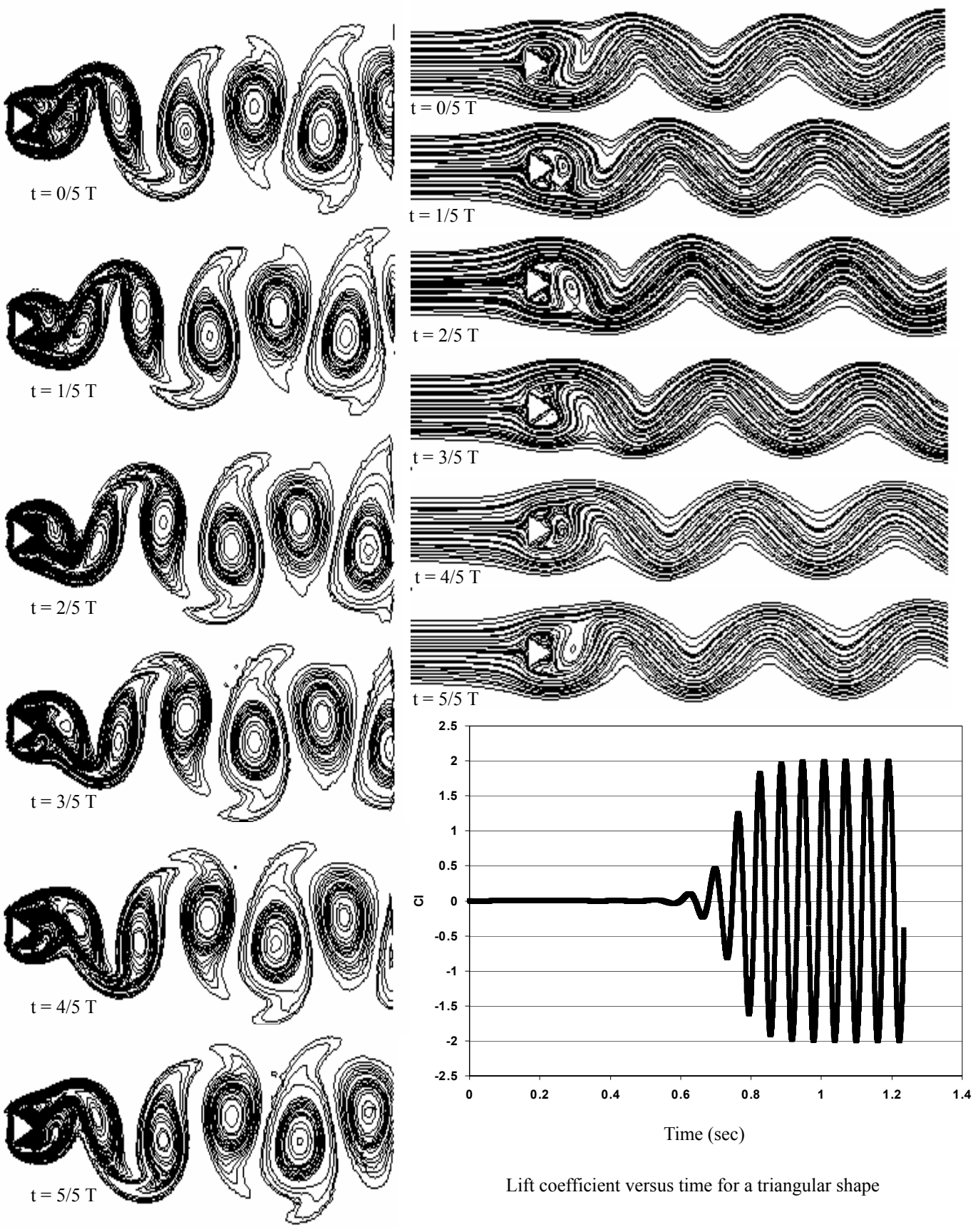

Figure 9. Time evolution of vortex shedding streamlines and vorticity magnitude for flow passing a triangular shape cylinder at Re = 100

Lift coefficient versus time for a triangular shape

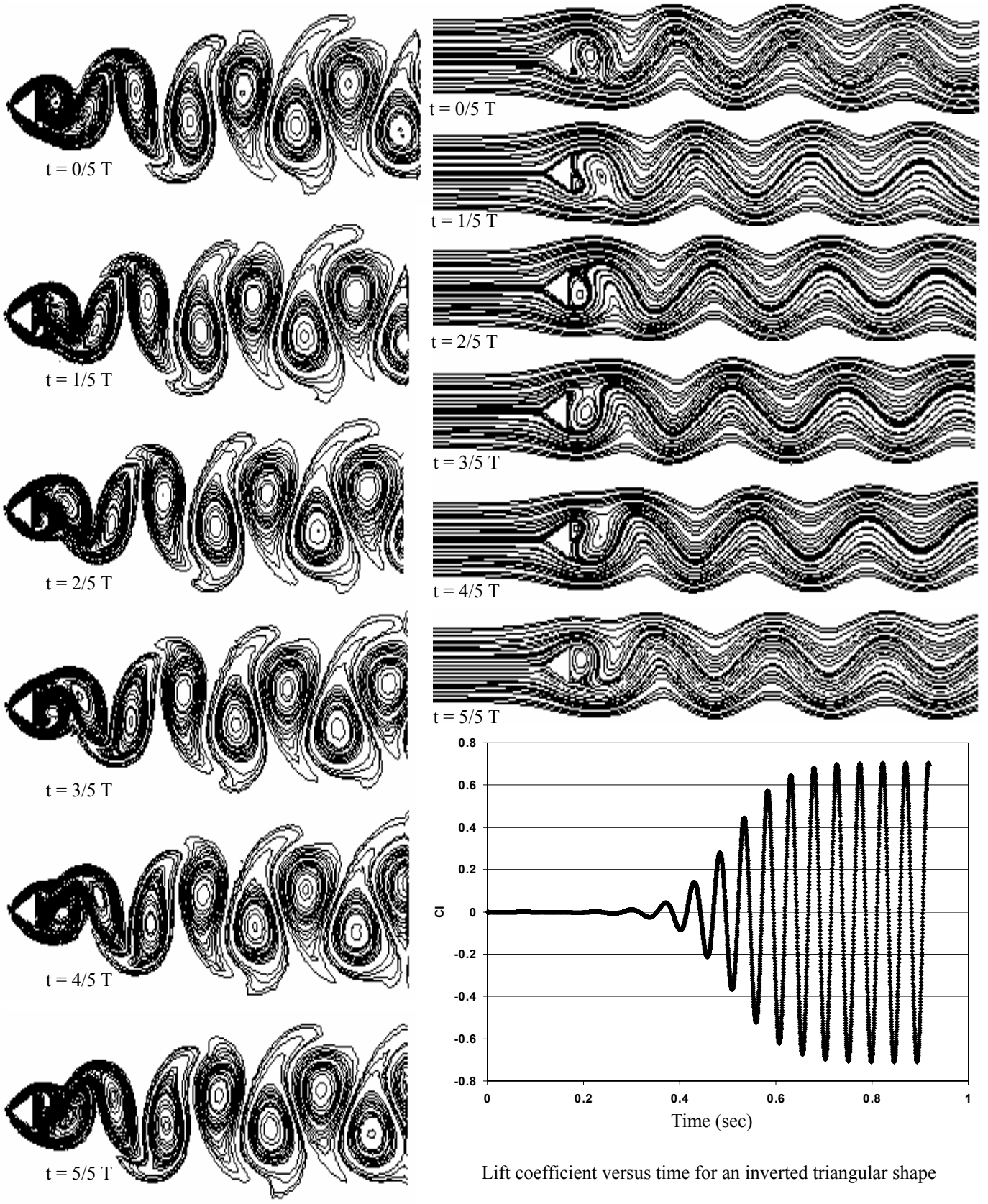

Lift coefficient versus time for an inverted triangular shape

Figure 10. Time evolution of vortex shedding streamline plots and vorticity contours for flow passing an inverted triangular shape cylinder at Re = 100

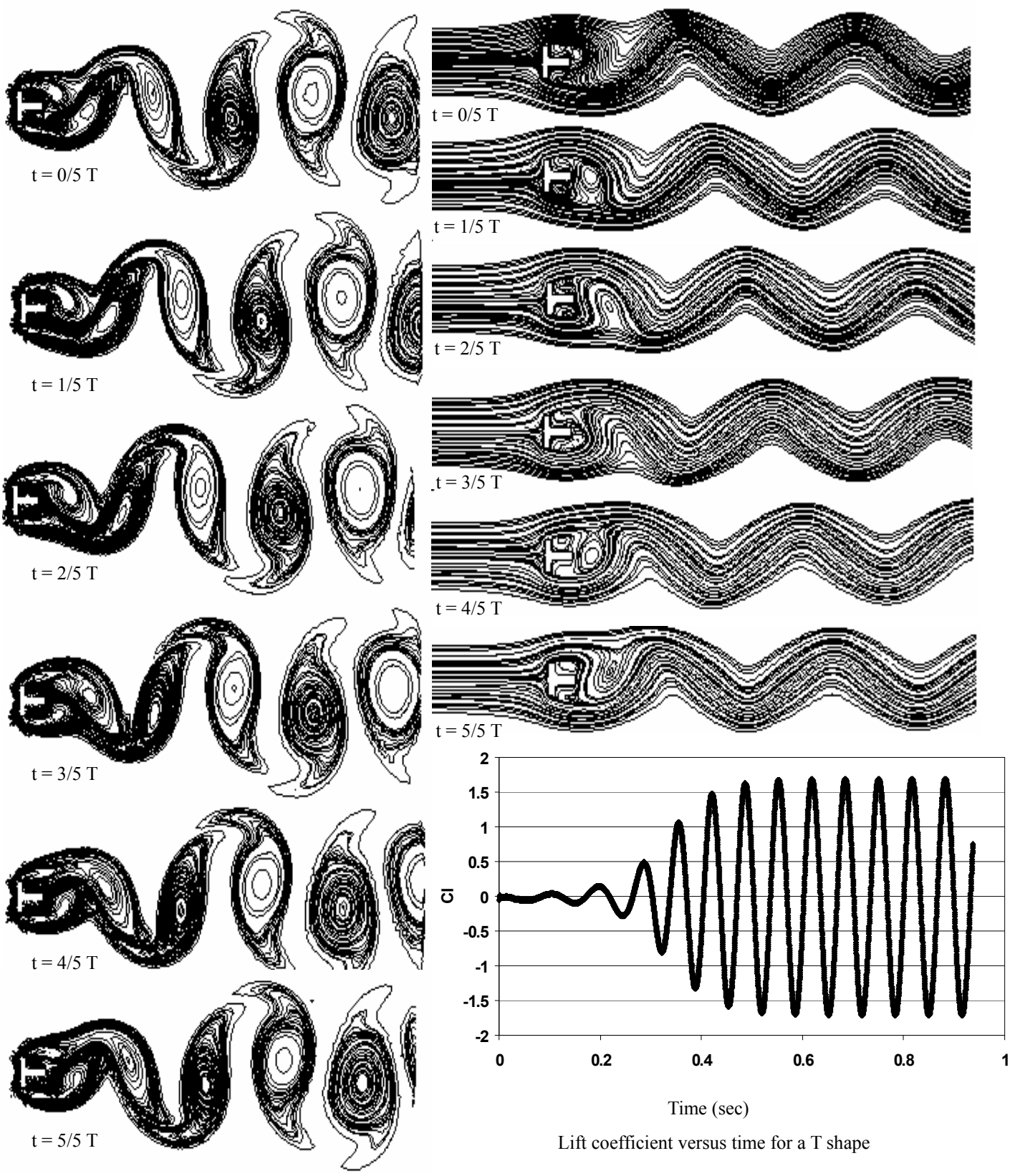

Figure 11. Time evolution of vortex shedding streamline plots and vorticity contours for flow passing a T-shape cylinder at Re = 100

Lift coefficient versus time for a T shape

CONCLUSION

Steady and unsteady flows past bluff bodies were simulated in the present study. For the range $Re \leq 200$ there are two distinct regimes, a laminar steady regime and a laminar unsteady regime. In the laminar steady regime, a pair of vortices appears in the wake of the body. These vortices are perfectly symmetric and increase in length with increasing Reynolds number. The gradient by which the recirculation length increases with respect to Reynolds number is shown to depend on the bluff body geometry. In the laminar unsteady regime, vortex shedding appears which has a perfect periodicity for the studied shapes. This has been shown using streamline plots and vorticity contours. The inverted triangular cylinder has the largest Strouhal number (St = 0.21) at Re = 100 while the T shaped cylinder has the smallest Strouhal number (St = 0.1516). Meanwhile, at Re = 200 the square cylinder has the smallest Strouhal number (St = 0.156). Moreover, the values of the critical Reynolds number for all shapes are considerably close to each other.

REFERENCES

1- Sohankar, A., Norberg, C., Davidson, L., "Numerical simulation of unsteady flow around a square two-dimensional cylinder", Twelfth Australaian Fluid Mechanics Conference, The University of Sydney, Australia 1995.

2- Sohankar, A., Norberg, C., Davidson, L., "A numerical study of unsteady two-dimensional flow around rectangle cylinders at incidence", International report Nr. 96/25. Department of Thermo and Fluid Dynamic Chalmers University of Technology at Gothenburg, Sweden, May 1996.

3- Sohankar, A., Norberg, C., Davidson, L., "Low-Reynolds-number flow around a square cylinder at incidence: study of blockage, onset of vortex shedding and outlet boundary condition", International Journal for Numerical Methods in Fluids, VOL. 26, 1998.

4- Young, D.L., Huang, J.L., Eldho, T.I., "Simulation of laminar vortex shedding flow past cylinders using a coupled of BEM and FEM model", Comput Methods Appl. Mech. Engrg. 190, 2001.

5- Ding, H., Shu, C., Yeo, K.S., Xu, D., "Simulation of incompressible viscous flows past a circular cylinder by hybrid FD scheme and meshless least square-based finite difference method", Comput. Methods Appl. Mech. Engrg. 193, 2004.

6- Frank, S., Xin, F., Ying, C., "Effect of pressure unsteadiness on vortex shedding frequency from dual bluff body", supported by SRF for ROCS, SEM and Zhejiang Provincial Natural Science Foundation (599086), University PHD Discipline Foundation of Chinese Education Ministry (2000033501).

7- Miau, J. J., Yang, C. C., Chou, J. H., Lee, K. R., "A T-shaped vortex shedder for a vortex flowmeter", Flow Meas. Instrum., 1993 Vol 4 No 4.

8- Mittal, S., Kumar, V., Raghuvanshi, A., "Unsteady incompressible flows past two cylinders in tandem and staggered arrangements", International Journal for Numerical Methods in Fluids, vol. 25, 1997.

9- Sumner, D., Price, S.J., Pafdoussis, M.P., "Flow-pattern identification for two staggered circular cylinders in cross-flow", J. Fluid Mech., vol. 411, 2000.

10- Sumner, D., Richards, M. D., Heseltine, J. L., "Mean aerodynamic forces acting on a pair of circular cylinders in cross-flow", American Institute of Aeronautics and Astronautics, AIAA 2001-2850.

11- Sohankar, A., Norberg, C., Davidson, L. "Numerical simulation of flow past a square cylinder", 3rd ASME/JSME Joint Fluids Engineering Conference, July 1999, San Francisco, California, USA.

12- Kim, D.H., Yang, K.S., Senda, M., "Large eddy simulation of turbulent flow past a square cylinder confined in a channel", Computers & Fluids 33, 2004.

13- S.C.R., Dennis, G.Z., "Chang, Numerical solutions for steady flow past a circular cylinder at Reynolds numbers up to 100", J. Fluid Mech. 42, 1970.

14- H. Takami, H.B. Keller, "Steady two-dimensional viscous flow of an incompressible fluid past a circular cylinder", Phys. Fluids 12 (Suppl. II) (1969) II-51.

15- S.Y. Tuann, M.D. Olson, "Numerical studies of the flow around a circular cylinder by a finite element method", Comput. Fluids 6 (1978) 219.

16- B. Fornberg, "A numerical study of steady viscous flow past a circular cylinder", J. Fluid Mech. 98 (1980) 819.

17- Hu, G.H., Sun, D.J., Yin, X.Y., Tong, B.G., " Hopf bifurcation in wakes behind a rotating and translating circular cylinder", Physics of Fluids, 1996.

18- Sohankar, A., Norberg, C., Davidson, L., "Numerical simulation of unsteady low-Reynolds number flow around a rectangular cylinder at incidence", Proc. 3rd Int. Colloq. on Bluff Body Aerodynamics and Applications, VA, 1996.

19- Kelkar, K. M., Patankar, S. V., "Numerical prediction of vortex shedding behind a square cylinder", Int. J. numer. meth. Fluids, 14, 327 (1992).

20- Kumar De, A., Dalal, A., "Numerical simulation of unconfined flow past a triangular cylinder", 2006 John Wiley & Sons, Ltd.

21- Grosho, P.M., S.T., Chan. Lee, R.L., Upson, C.D., " A modified finite element method for solving the time dependent, incompressible Navier-Stokes equations part 2: application, Int. J. Numer. Methods Fluids 4, 1984.

22- Li, J., Chambarel, M., Donneaud, M., Martin, R., " Numerical study of laminar flow past one and two circular cylinders", Comput. Fluids 19 (2), 1991.

23- Braza, M., Chassaing, H.H. Minh, "Numerical study and physical analysis of the pressure and velocity fields in the near of a cylinder", J. Fluid Mech. 165, 1986.

24- White, M.W., “Fluid Mechanics”, McGraw-Hill companies, united state of America, 1999, fourth edition
25- Jan, Y.J., Sheu, T. W.H., “A numerical confirmation of the dual body vortex flow meter design”, Computers & Fluids 33, 2004.
26- Okajima, A., “Strouhal number of rectangular cylinders”, J. Fluid Mech., 1982.
27- Davis, R.W., Moore, E.F., Purtell, L.P., “ A numerical experimental study of confined flow around rectangular cylinders”, Phys of Fluids, 1984.